Int J Adv Manuf Technol (2016) 84:261–273
DOI 10.1007/s00170-015-8066-2

ORIGINAL ARTICLE

Design and manufacturing model of customized hydrostatic bearing system based on cloud and big data technology

Zhifeng Liu[1] · **Yumo Wang**[1] · **Ligang Cai**[1] · **Qiang Cheng**[1] · **Haiming Zhang**[1]

Received: 20 May 2015 / Accepted: 30 October 2015 / Published online: 11 November 2015

Abstract Hydrostatic systems are considered as essential supporting structures in heavy machine tools. The calculations and analyses for hydrostatic bearings are always laborious because of the involvement of several disciplines such as elastic mechanics, hydromechanics, thermodynamics, and other factors in the design. It is well known that large data and cloud technology are capable of processing and transmission of hydrostatic system studies. In this work, a cloud manufacture model is presented to provide big data storage, transmission, and processing platform for designers, manufacturers, and users of hydrostatic bearings. All participants involved in the manufacturing were linked together by timely information communication in order to ensure that the customized products met with the actual conditions in the cloud server. Based on the actual requirements of the user, the carrying capacity of hydrostatic system was analyzed by a designer using finite difference method and the results were sent to the manufacturer for machining of components. The monitored data from the consumer could be fed back to the designer for performance evaluation through the cloud server. It was found that customized manufacturing tasks could be finished more reliably and efficiently if all participants exchanged the data through cloud platform in real time.

Keywords Hydrostatic bearing system design · Cloud manufacture model · Customized processing · Big data · FDM

✉ Zhifeng Liu
lzfbjut@gmail.com

Yumo Wang
wangyumo@emails.bjut.edu.cn

Ligang Cai
lgai321@aliyun.com

Qiang Cheng
chengqiangbjut@sina.cn

Haiming Zhang
hbkjzhm@163.com

[1] College of Mechanical Engineering and Applied Electronics Technology, Beijing University of Technology, 100124 Beijing, People's Republic of China

1 Introduction

Cloud manufacturing which is a new concept provides platform for participant's interactions to facilitate the manufacturing and production more environmental friendly and efficient [1, 2]. Computer-integrated manufacturing (CIM), collaborative manufacturing network, and industrial product–service system (IPS^2) are regarded as typical examples of cloud manufacture which benefits the production a lot [3, 4]. Timely information interchange is essential for socialized production, which demands a service-oriented manufacturing model [5–7]. Manufacture processes become more cost-effective, flexible, and scalable with the help of cloud and big data technologies, which is the foundation of service-oriented or customized manufacturing [8, 9]. The computing speed and data processing ability of the network server was developed to a high level to ensure the machine tool production to be more effective and dependable [10–12]. Hydrostatic systems are widely used in supporting structures of heavy machine tools because of their less wear and large carrying capacity. The performance of hydrostatic bearing is highly associated with the design and quality of manufacturing of its parts. [13] Because hydrostatic bearings are always used in special machine tools of large size, bearing systems users usually preferred customized design and manufacture, which not only requires manufacturing but also services-oriented model [6]. A film thickness, which is usually designed for less than

100 μm, is used to support the surfaces loaded with several hundred of tons, so even slight geometrical errors could influence the bearing performance [14]. Three participants of different specializations are involved in the manufacture of hydrostatic systems namely, the designer, manufacturers, and user who may be located in different cities or even countries. The exchange of communications between various members in the manufacturing model would be more efficient if transfer of information occurred through a cloud platform [15, 16]. The Reynolds equation is widely used in hydrostatic system analyses to describe the pressure distribution in oil pads which is necessary to solve the load-carrying capacity of the bearings [17–19]. According to the requirements specified by the consumer, the designer is required to modify the Reynolds equation to match the actual working conditions of hydrostatic bearings [20, 21]. According to the multi-body system (MBS) theory, the tool tip position is significantly affected by the small errors [22, 23]. In addition, the design value of the film thickness is usually less than 100 μm, so the geometrical tolerances such as surface roughness, waviness, or shape error strongly influence the bearing performance [24, 25]. There are numerous types of geometrical errors which could only be observed and measured during manufacturing. It is of advantage if this information is sent by the manufacturers to the designer for ensuring reliability. With the help of the strong data processing or transmitting ability and optimization algorithms, the production demands are being fulfilled [26]. Hydrostatic bearing users group is growing rapidly with the developing cloud server technology. The cloud manufacture model can be applied at multiple occasions since all participating members can join every phase of the manufacture [27]. A computational platform with high speed and convenience is provided to the designer for analyzing the structure numerically [28, 29]. By using the finite-difference method (FDM), the numerical results of carrying capability could be determined after pressure resolution. The numerical method is dependable, but it increases the amount of computing which however is compensated by the large data handling capacity of the cloud server [30, 31]. With optimal algorithm of cloud computing, the manufacturing resources can be reallocate more effectively in the whole production [15, 32, 33]. After the manufacture of hydrostatic bearing, the monitoring data also provides feedback through cloud platform to the designer for performance evaluation [34, 35].

In this paper, a customized cloud manufacture model for hydrostatic bearings is presented. The designer is required to establish a modified Reynolds equation which takes the film thickness variation into consideration according to the requirements of the consumer. The pressure distribution which can be determined by numerical method is then integrated to obtain carrying capacity. The actual surface roughness, waviness, and shape error measured during manufacture should be taken into consideration in the design and analysis. Based on the real conditions, the theoretical working performance will be more dependable. The cloud platform is the foundation of information exchange between the designer and manufacturer separated by distance. Cloud server is demanded to handle and transfer big data, because the geometric errors of multiple batches or numerical method being used in the resolution have a large data for calculations. In addition, the numerical results in any step of cloud manufacture may be used for further analyzing or debugging, so they are needed to be stored appropriately instead of caching. A big data storage ability of cloud platform is also in need. The machining criterion for manufacturer is determined by the designer based on theoretical analysis. Through the customized cloud manufacture model, the monitoring data from the consumer is sent as

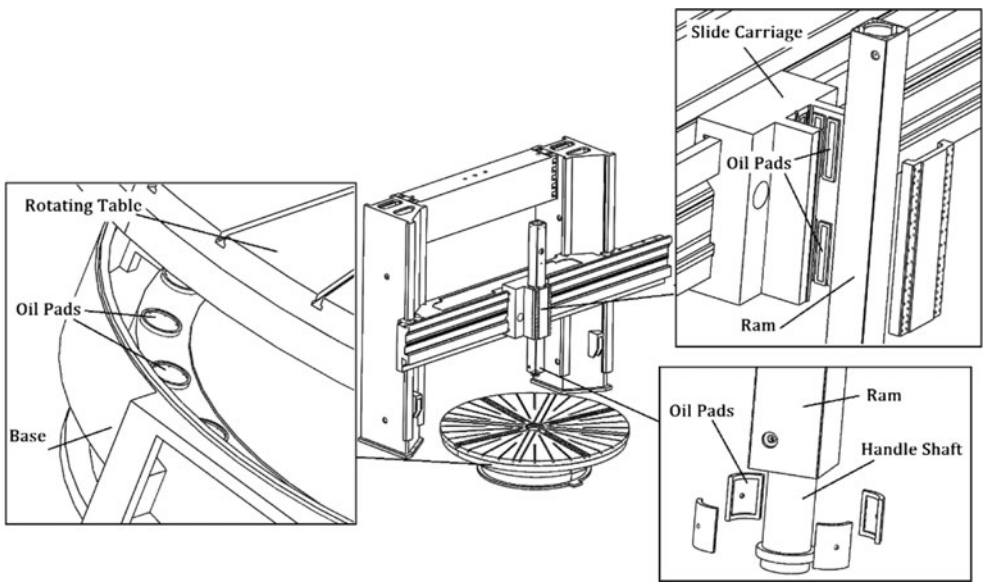

Fig. 1 Milling machine with hydrostatic bearings

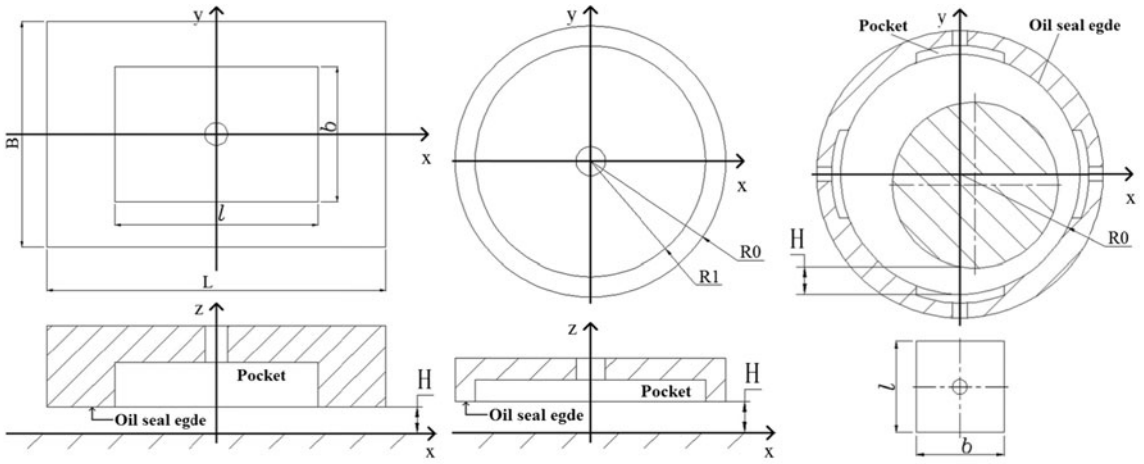

(a) Oil pad for rectangular bearing (b) Oil pad for Circular bearing (c) Oil pad for Journal bearing

Fig. 2 Models of oil pads. **a** Oil pad for rectangular bearing. **b** Oil pad for circular bearing. **c** Oil pad for journal bearing

feedback to the designer for performance assessment or for record of previous cases.

2 Hydrostatic bearing design

2.1 Common application of hydrostatic systems in machine tools

There are three types of oil pads which are used by hydrostatic bearings: rectangular, circular, and journal, and their operating principles are similar. The pressure from the lubricating oil pumped into the oil pockets of oil pads generates the major part of load-carrying capacity. Then the pressure within oil pockets is maintained by the hydrostatic effect caused by the flow of oil in the seal edge. The rectangular, circular, and journal oil pads are applied to the different parts of the machine tools for specialized supporting and lubricating duties.

A common type of multiple-axis milling machine is shown in Fig. 1. It can be seen that its rotating platform, slider carriage, and shaft are supported by hydrostatic bearing. The rectangular bearing is used in linear rail such as slider carriage and ram; circular bearing is used in rotary rail such as rotating table; journal bearing is used in radial support such as handle shaft. The essential features of the three types of oil pads are shown in Fig. 2.

In Fig. 2, L is the length of oil pad, B is the width of oil pad (or R0 is the radius of oil pad), l is the length of oil pocket, b is the width of oil pocket (or R1 is the radius of oil pocket), and H is the thickness of oil film.

As the theoretical computational method of hydrostatic systems used in cloud manufacture model is applied to several customized machine tools on a distinct scale, it is necessary that all parameters considered here are made dimensionless in order to make them versatile and more general.

$$\begin{gathered}\overline{p}=\frac{p}{p_0},\overline{p_0}=1,\overline{x}=\frac{x}{L},\overline{L}=1,\overline{y}=\frac{y}{B},\overline{B}=1,\overline{r}=\frac{r}{R_0},\overline{R_0}=1,\overline{h}=\frac{h}{H_0},\overline{H_0}=1,\\ \overline{U}=\frac{U}{\frac{H_0^2p_0}{L\eta}}\left(or\,\overline{U}=\frac{U}{\frac{H_0^2p_0}{R_0\eta}}\right),\overline{W}=\frac{W}{LBp_0}\left(or\,\overline{W}=\frac{W}{R_0Bp_0}\right),\overline{M}=\frac{M}{L^2Bp_0}\left(or\,or\,\overline{M}=\frac{M}{R_0^2Bp_0}\right),\\ \overline{q}=\frac{q}{\frac{H_0^3p_0}{\eta}}\end{gathered}\tag{1}$$

where, p is oil pressure, p_0 is pressure in the oil pocket, W is carrying capacity, q is volumetric flow rate, U is velocity, h is film thickness, and η is viscosity. In addition, $\overline{p}$ is dimensionless pressure, $\overline{x}$ is dimensionless length on x coordinate, $\overline{y}$ is dimensionless length on y coordinate, $\overline{W}$ is dimensionless carrying capacity, $\overline{M}$ is dimensionless moment, $\overline{q}$ is dimensionless flow rate, $\bar{U}$ is dimensionless velocity, and $\overline{h}$ is dimensionless film thickness.

2.2 Establishment and solving the Reynolds equation

The carrying ability analysis is considered as a key process in hydrostatic systems cloud manufacture model, and the designer has to establish a general method that it can be applied in different circumstances. The Reynolds equation is extensively used in research studies to examine the carrying capacity. The solution to Reynolds equation in this particular case is the pressure distribution in oil pad. Based on the integration of pressure distribution, the supporting capacity can be determined and the dynamic performances like stiffness or damping can also to be solved by additional computations. The reliability of the Reynolds equation has been verified and reported in literature which proves that it be widely applied. The Reynolds equation for rectangular, circular, and journal bearing can be expressed in the following forms [13]:

$$\begin{aligned}
\text{rectangular bearing}: &\frac{\partial}{\partial \bar{x}}\left(\bar{h}^3\cdot\frac{\partial \bar{p}}{\partial \bar{x}}\right)+\left(\frac{L}{B}\right)^2\frac{\partial}{\partial \bar{y}}\left(\bar{h}^3\cdot\frac{\partial \bar{p}}{\partial \bar{y}}\right)=6\frac{\partial}{\partial \bar{x}}\left(\overline{U_x}\bar{h}\right)+6\frac{\partial}{\partial \bar{y}}\left(\overline{U_y}\bar{h}\right)\\
\text{circular bearing}: &\frac{\partial}{\partial \bar{r}}\left(\bar{r}\cdot\bar{h}^3\cdot\frac{\partial \bar{p}}{\partial \bar{r}}\right)+\frac{\partial}{\partial \bar{\vartheta}}\left(\bar{h}^3\cdot\frac{\partial \bar{p}}{\bar{r}\partial \bar{\vartheta}}\right)=6\frac{\partial}{\partial \bar{r}}\left(\bar{r}\overline{U_r}\bar{h}\right)+6\frac{\partial}{\partial \bar{\vartheta}}\left(\overline{U_\vartheta}\bar{h}\right)\\
\text{journal bearing}: &\frac{\partial}{\partial \bar{\phi}}\left(\bar{h}^3\cdot\frac{\partial \bar{p}}{\partial \bar{\phi}}\right)+\left(\frac{R_0}{L}\right)^2\frac{\partial}{\partial \bar{y}}\left(\bar{h}^3\cdot\frac{\partial \bar{p}}{\partial \bar{y}}\right)=6\frac{\partial}{\partial \bar{\phi}}\left(\overline{U_\phi}\bar{h}\right)+6\frac{\partial}{\partial \bar{y}}\left(\overline{U_y}\bar{h}\right)
\end{aligned}\tag{2}$$

In the equations, $\overline{\vartheta}$ is the angle coordinate for circular bearing and $\overline{\phi}$ is the angle coordinate for journal bearing.

Partial differential equations shown as Eq. 2 are complicated to solve analytically. However, by using a numerical method, they can be transformed into algebraic equations, which are relatively easier to solve. The continuous Reynolds equations are transformed to discrete equations approximately, which then can be solved by Gauss–Seidel iteration and successive over-relaxation (SOR) computational acceleration. The pressure distribution can be determined by solving the Reynolds equations. The numerical methods have been widely used in resolving intricate differential equations but such approach increases the amount of computations dramatically, creating the big data demand from cloud manufacture model. Using FDM, the Reynolds equations in Eq. 2 are reorganized into discrete iterative equations [24] as shown by Eq. 3:

$$\begin{aligned}
&\text{rectangular bearing}:\\
&\bar{p}_{i,j}=\frac{\left[\begin{array}{l}\bar{y}^2_{\text{step}}\bar{h}^3_{i,j}\bar{p}_{i+1,j}+\bar{y}^2_{\text{step}}\bar{h}^3_{i-1,j}\bar{p}_{i-1,j}+\left(\frac{L}{B}\right)^2\bar{x}^2_{\text{step}}\bar{h}^3_{i,j}\bar{p}_{i,j+1}+\left(\frac{L}{B}\right)^2\bar{x}^2_{\text{step}}\bar{h}^3_{i,j-1}\bar{p}_{i,j-1}\\ +6\left(\overline{Ux}_{i,j}\bar{h}_{i,j}-\overline{Ux}_{i-1,j}\bar{h}_{i-1,j}\right)\bar{x}_{\text{step}}\bar{y}^2_{\text{step}}+6\left(\overline{Uy}_{i,j}\bar{h}_{i,j}-\overline{Uy}_{i,j-1}\bar{h}_{i,j-1}\right)\bar{x}^2_{\text{step}}\bar{y}_{\text{step}}\end{array}\right]}{\bar{y}^2_{\text{step}}\bar{h}^3_{i,j}+\bar{y}^2_{\text{step}}\bar{h}^3_{i-1,j}+\left(\frac{L}{B}\right)^2\bar{x}^2_{\text{step}}\bar{h}^3_{i,j}+\left(\frac{L}{B}\right)^2\bar{x}^2_{\text{step}}\bar{h}^3_{i,j-1}}\\
&\text{circular bearing}:\\
&\bar{p}_{i,j}=\frac{\left[\begin{array}{l}\bar{\vartheta}^2_{\text{step}}\bar{r}_i\bar{h}^3_{i,j}\bar{p}_{i+1,j}+\bar{\vartheta}^2_{\text{step}}\bar{r}_{i-1}\bar{h}^3_{i-1,j}\bar{p}_{i-1,j}+\bar{r}^2_{\text{step}}\bar{h}^3_{i,j}\bar{p}_{i,j+1}\Big/\bar{r}_i+\bar{r}^2_{\text{step}}\bar{h}^3_{i,j-1}\bar{p}_{i,j-1}\Big/\bar{r}_i\\ +6\left(\overline{Ur}_{i,j}\bar{h}_{i,j}-\bar{r}_{i-1}\overline{Ur}_{i-1,j}\bar{h}_{i-1,j}\right)\bar{r}_{\text{step}}\bar{\vartheta}^2_{\text{step}}+6\left(\overline{U\vartheta}_{i,j}\bar{h}_{i,j}-\overline{U\vartheta}_{i,j-1}\bar{h}_{i,j-1}\right)\bar{r}^2_{\text{step}}\bar{\vartheta}_{\text{step}}\end{array}\right]}{\bar{\vartheta}^2_{\text{step}}\bar{r}_i\bar{h}^3_{i,j}+\bar{\vartheta}^2_{\text{step}}\bar{r}_{i-1}\bar{h}^3_{i-1,j}+\bar{x}^2_{\text{step}}\bar{h}^3_{i,j}\Big/\bar{r}_i+\bar{x}^2_{\text{step}}\bar{h}^3_{i,j-1}\Big/\bar{r}_i}\\
&\text{journal bearing}:\\
&\bar{p}_{i,j}=\frac{\left[\begin{array}{l}\bar{y}^2_{\text{step}}\bar{h}^3_{i,j}\bar{p}_{i+1,j}+\bar{y}^2_{\text{step}}\bar{h}^3_{i-1,j}\bar{p}_{i-1,j}+\left(\frac{R_0}{L}\right)^2\bar{\phi}^2_{\text{step}}\bar{h}^3_{i,j}\bar{p}_{i,j+1}+\left(\frac{R_0}{L}\right)^2\bar{\phi}^2_{\text{step}}\bar{h}^3_{i,j-1}\bar{p}_{i,j-1}\\ +6\left(\overline{U\phi}_{i,j}\bar{h}_{i,j}-\overline{U\phi}_{i-1,j}\bar{h}_{i-1,j}\right)\bar{x}_{\text{step}}\bar{y}^2_{\text{step}}+6\left(\overline{Uy}_{i,j}\bar{h}_{i,j}-\overline{Uy}_{i,j-1}\bar{h}_{i,j-1}\right)\bar{x}^2_{\text{step}}\bar{y}_{\text{step}}\end{array}\right]}{\bar{y}^2_{\text{step}}\bar{h}^3_{i,j}+\bar{y}^2_{\text{step}}\bar{h}^3_{i-1,j}+\left(\frac{R_0}{L}\right)^2\bar{\phi}^2_{\text{step}}\bar{h}^3_{i,j}+\left(\frac{R_0}{L}\right)^2\bar{\phi}^2_{\text{step}}\bar{h}^3_{i,j-1}}
\end{aligned}\tag{3}$$

In Eq. 3, $\bar{x}_{\text{step}}$ is the step interval for the x coordinate, $\bar{y}_{\text{step}}$ is the step interval for the y coordinate, $\overline{\vartheta}_{\text{step}}$ is the step length for the ϑ coordinate, $\overline{\phi}_{\text{step}}$ is the step length for the ϕ coordinate, and i and j are numerical counts of the elements.

The boundary conditions for iterative equation should be set clearly before solving by Gauss–Seidel method. According to the oil pad model shown in Fig. 2, pressure in oil pocket is set as 1 because it is filled with pressurized oil and pressure at the outer boundary of oil seal edge is set as 0 because it pressures at the outlet. The boundary conditions can be written as:

$$\begin{aligned}
\text{rectangular bearing}: \bar{p}_{i,j}&=\begin{cases}1, \left|\bar{x}_i\right|<\frac{1}{2}\bar{l}\ \text{and}\left|\bar{y}_i\right|<\frac{1}{2}\bar{b}\\ 0, \left|\bar{x}_i\right|=\frac{1}{2}\bar{L}\ \text{or}\left|\bar{y}_i\right|=\frac{1}{2}\bar{B}\end{cases}\\
\text{circular bearing}: \bar{p}_{i,j}&=\begin{cases}1, \left|\bar{r}_i\right|<\bar{R}_1\\ 0, \left|\bar{r}_i\right|=\bar{R}_1\end{cases}\\
\text{journal bearing}: \bar{p}_{i,j}&=\begin{cases}1, \left|\overline{R}_0\bar{\phi}_i\right|<\frac{1}{2}\bar{b}\ \text{and}\left|\bar{y}_j\right|<\frac{1}{2}\bar{l}\\ 0, \ \left|\bar{y}_j\right|=\frac{1}{2}\bar{L}\end{cases}
\end{aligned}\tag{4}$$

The carrying capacity can be determined by obtaining solution to pressure distribution. The numerical integration could be used to solve the double integral for obtaining the discrete pressure results at each node on x and y coordinate axes. The discrete nodes are shown in Fig. 3:

The expression for numerical integration can be written as:

$$\overline{W}=\sum\frac{1}{4}\left(\bar{p}_{i,j}+\bar{p}_{i+1,j}+\bar{p}_{i,j+1}+\bar{p}_{i+1,j+1}\right)\cdot\bar{x}_{\text{step}}\cdot\bar{y}_{\text{step}}\tag{5}$$

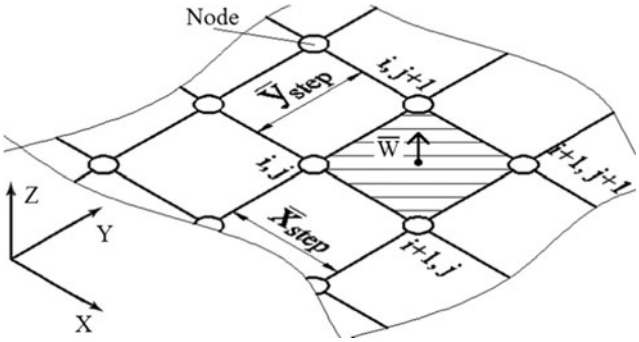

Fig. 3 Numerical integration on discrete nodes

According to Eq. 1, the carrying capacity can be determined by oil supply flow rate and the geometry of structure of the oil pad [23].

$$W = \begin{cases} \dfrac{\overline{W}LB\eta}{\overline{q}H_0^3}\cdot Q_e, \text{rectangular bearing} \\ \dfrac{\pi\overline{W}R_0^2\eta}{\overline{q}H_0^3}\cdot Q_e, \text{circular bearing} \\ \dfrac{2\pi\overline{W}LR_0\eta}{\overline{q}H_0^3}\cdot Q_e, \text{journal bearing} \end{cases} \quad (6)$$

In Eq. 6, Q_e is the supply oil volumetric flow rate through each oil pad.

3 Cloud manufacturing model for hydrostatic systems

The carrying ability of hydrostatic bearings can be strongly influenced by geometrical errors. However, the geometrical flaws such as surface roughness, waviness, or shape error occurring during manufacturing are difficult to avoid and can only be observed by specialized devices after machining process. The component manufactures of hydrostatic systems who could measure the geometrical errors are unable to carry out further analysis. The designers are frequently hindered by limitation of funds to build their own experimental or measurement platform. To overcome this problem, a new type of manufacturing model with timely information exchange platform is needed to link the designer and manufacturer in order to improve the reliability and efficiency of the bearing production processes. The customized hydrostatic system cloud manufacture model is based on the carrying capacity analysis which is the standard for evaluation of the structure design. In addition, the design should be capable of being adjusted to match the actual working conditions with the geometrical error measured by the component manufacturer. After assembly, the hydrostatic bearing can be tested by the manufacturer and the experimental data could be sent to the designer for verification. The machine tool will be monitored after the delivery. The data sent to the designer will stand as a source for performance evaluation or reliability confirmation. The cloud manufacture is entirely based on network server to provide the designer, manufacturer, and consumer a channel for exchange of information and communications.

Figure 4 shows that cloud server supports timely communications between all the participants in hydrostatic system manufacture to make the customized products more reliable. The functional or performance specifications and monitoring data should be provided by the consumer. The design based on previous work or analysis based on theoretical calculations should be

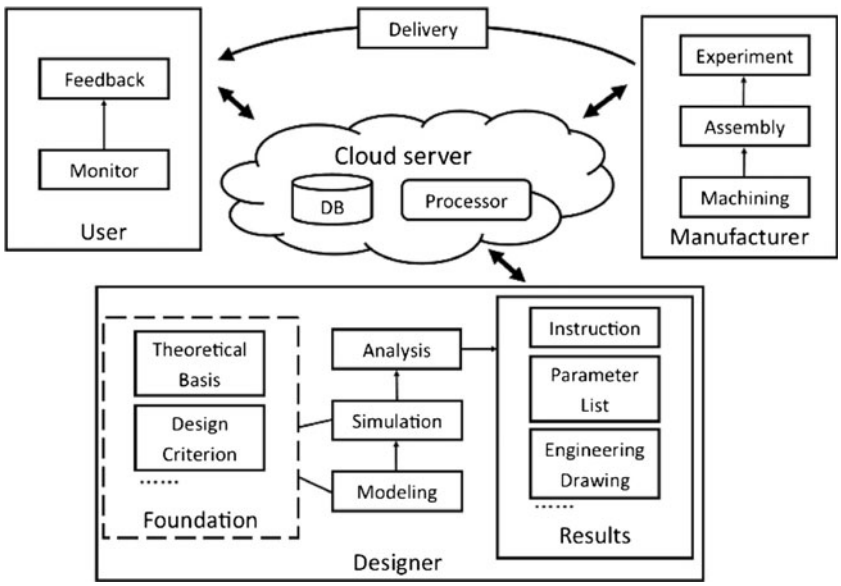

Fig. 4 Cloud server for designer, manufacturer, and user [1]

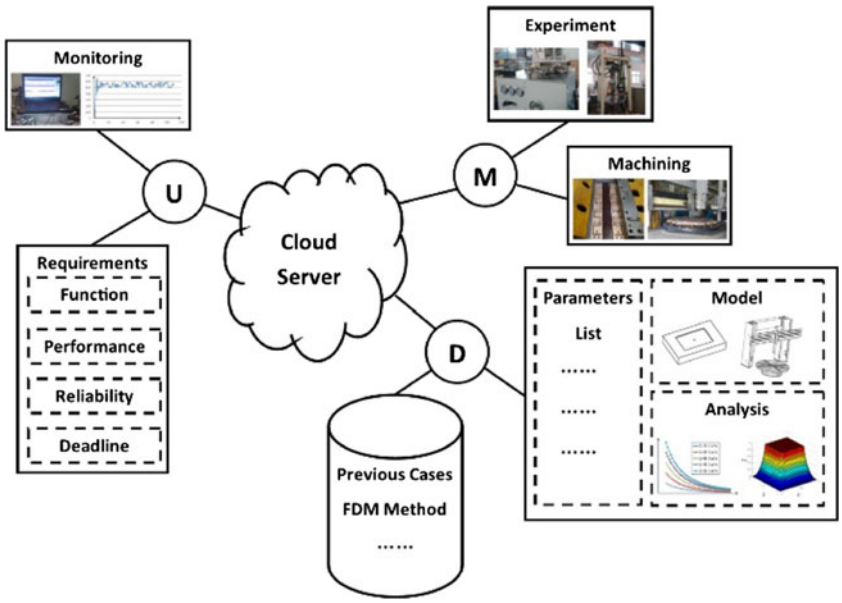

Fig. 5 Simplified topology of the model for cloud manufacture [21]

offered by the designer to the manufacturer for determining the machining demands or analyzing reports. The experimental data and processing schedules should be offered by the manufacturer in real time.

In Fig. 5, U stands for user, D stands for designer, and M stands for manufacturer. In the general modeling process, the designer is required to complete the prototype model of hydrostatic bearings according to the specifications received from the user. In the machining progress, the manufacturer has to complete the machining of the essential parts of hydrostatic systems such as oil pads based on the model determined by designer and send the measurement data back to the designer. In analyzing the process, the designer should analyze the predicted performance according to the geometrical error data and FDM algorithm to ensuring that the bearing meets actual working conditions. Several corrections may have to be made to the prototype model to match the machining conditions. After the hydrostatic system is assembled in the machine tool, experiments are needed to establish the required adjustments and structural parameters which are required by the consumer to build the foundation and workshop. In the utilization stage, monitoring data could be fed back to the designer for

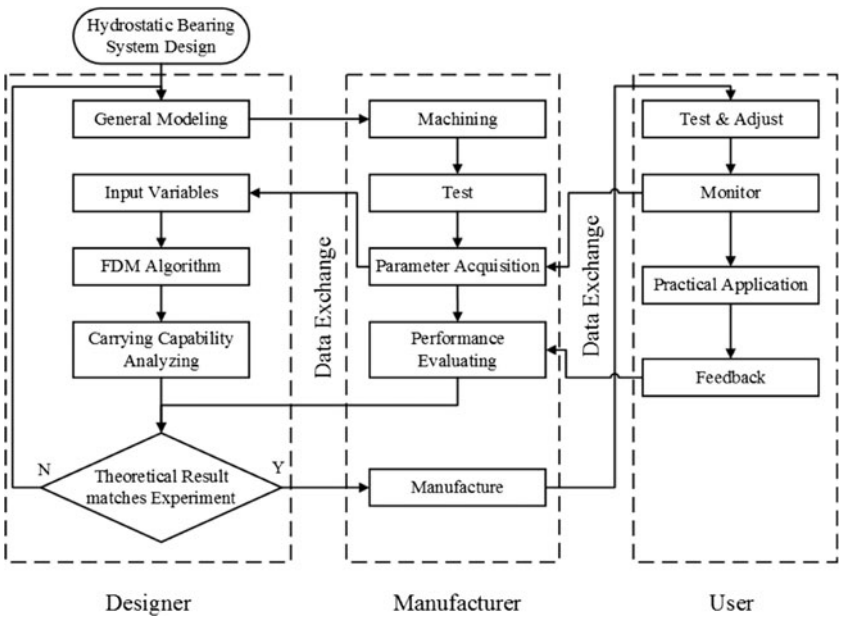

Fig. 6 Hydrostatic bearing system cloud manufacture process

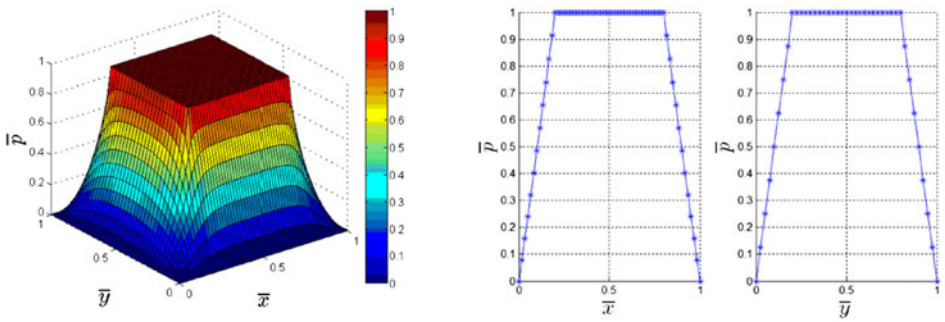

(a) Pressure distribution in oil pad of rectangular bearing

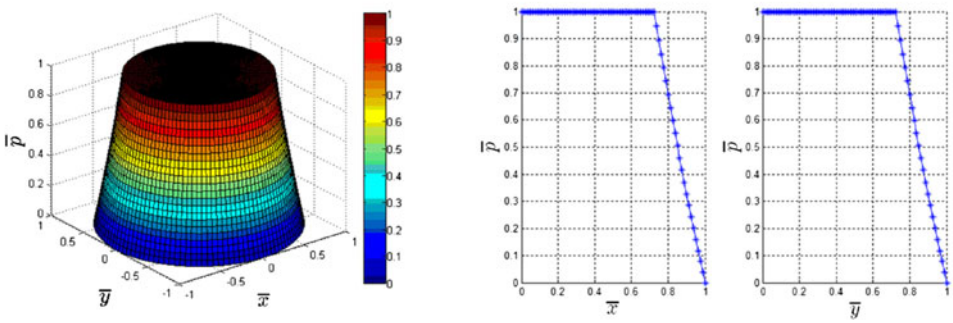

(b) Pressure distribution in oil pad of circular bearing

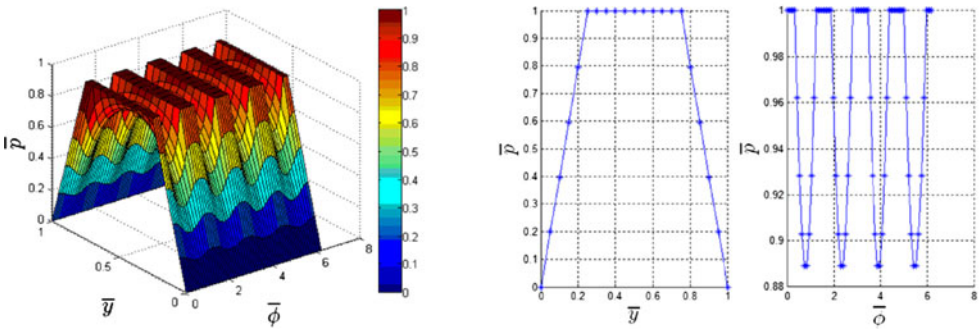

(c) Pressure distribution in oil pad of journal bearing

Fig. 7 Dimensionless pressure distribution in oil pads. **a** Pressure distribution in oil pad of rectangular bearing. **b** Pressure distribution in oil pad of circular bearing. **c** Pressure distribution in oil pad of journal bearing

performance assessment and to prepare the maintenance schedules or plans for upgrading (Fig. 6).

4 A case for application of cloud manufacturing of hydrostatic bearing

4.1 FDM solution to the Reynolds equation for hydrostatic bearing

FDM which is regarded as a common method easy to implement for analysis of bearing carrying ability analysis the advanced cloud server offers it an efficient computational platform to perform numerical computations. After algebraic discretion and Gauss–Seidel iteration, the pressure distribution results obtained for the three types of oil pads are shown in Fig. 7.

The pressure distribution in oil seal edge appears to be linear in all three types of oil pads, and the length and width of oil pocket can only be determined from the user functional requirements, namely through the cloud server. In machining, it is impossible to make the ideal model to be in agreement with the manufactured part. The geometrical tolerances like waviness or shape error need to be incorporated into the Reynolds equation to bring ideal model closer to the real working conditions. The carrying capacity of the oil pad will be strongly influenced by flatness among all kinds of shape errors, and it can be described by incorporating a linear function into the oil film

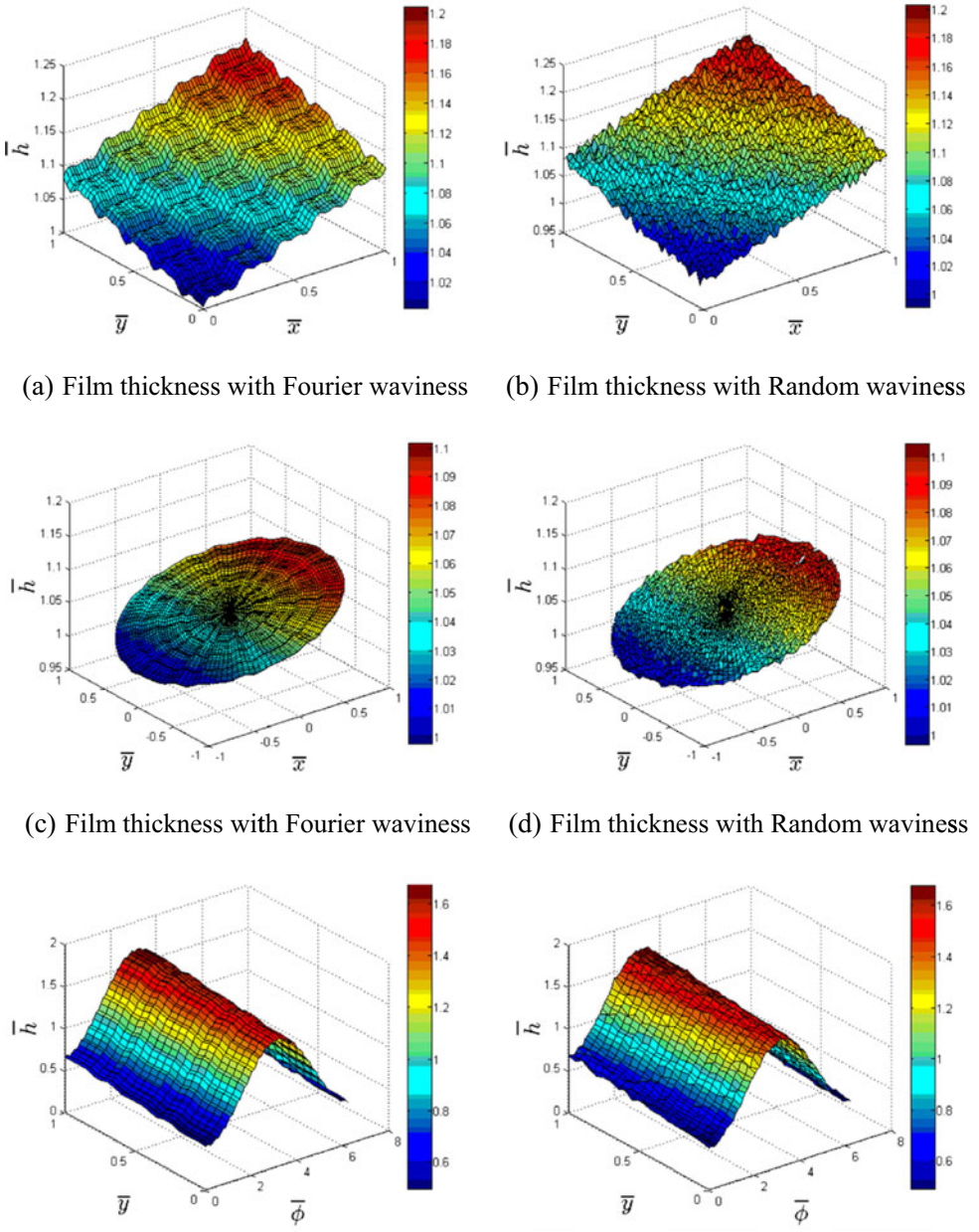

(a) Film thickness with Fourier waviness (b) Film thickness with Random waviness

(c) Film thickness with Fourier waviness (d) Film thickness with Random waviness

(e) Film thickness with Fourier waviness (f) Film thickness with Random waviness

Fig. 8 Dimensionless film thickness with geometric error. **a** Film thickness with Fourier waviness. **b** Film thickness with Random waviness. **c** Film thickness with Fourier waviness. **d** Film thickness with Random waviness. **e** Film thickness with Fourier waviness. **f** Film thickness with Random waviness

Table 1 Dimensionless pressure distribution data for the cloud platform

Dimensionless pressure distribution								
0	0	0	0	⋯	0	0	0	0
0	0.020124879	0.042270452	0.062095901	…	0.06021494	0.039691316	0.019543185	0
0	0.040071764	0.081983695	0.122870114	…	0.121267708	0.079817558	0.038662427	0
0	0.060641156	0.122948164	0.185124467	…	0.181363114	0.119433001	0.05837198	0
…	…	…	…	…	…	…	…	…
0	0.059179831	0.1197943	0.182474267	…	0.178193859	0.116388744	0.057480835	0
0	0.03988186	0.080025523	0.120703148	…	0.118599393	0.07830041	0.038088751	0
0	0.020060935	0.039995317	0.060024577	…	0.059031173	0.038104443	0.019015919	0
0	0	0	0	…	0	0	0	0

Table 2 Film thickness data for the cloud platform

Dimensionless film thickness								
1.0038443	1.0154956	0.9886159	1.013314	…	1.138505	1.13662	1.14860	1.13521
1.0014827	1.0075839	1.0138860	1.019441	…	1.135686	1.130847	1.16265	1.15015
1.0123596	0.9973173	1.0039160	1.007701	…	1.144513	1.130997	1.14637	1.13943
1.0013555	1.0100857	1.0159461	1.002908	…	1.131973	1.148659	1.14687	1.14654
…	…	…	…	…	…	…	…	…
1.0418857	1.0540743	1.0528358	1.052307	…	1.189604	1.193943	1.18316	1.18942
1.0463390	1.0455528	1.0542093	1.057214	…	1.1884577	1.176325	1.19260	1.180981
1.0478144	1.0380710	1.0573485	1.060853	…	1.189267	1.201029	1.195691	1.192354
1.0458922	1.0559565	1.0513053	1.058854	…	1.185507	1.177137	1.193791	1.186480

thickness. The waviness could be represented as a periodic function which can be approximated by Fourier expansion or a random variation which can be expressed as stochastic wave around the desired value. However, either type of the expressions of waviness can only be described by nodes with enough denseness. This is another reason why the cloud manufacturing platform requires a strong ability to process and transmit big data. The film thickness combined with geometric tolerance is shown in Fig. 8.

Figure 8a shows dimensionless film thickness of rectangular oil pad incorporated with Fourier waviness and linear slope on x and y coordinate axes; Fig. 8b is dimensionless film thickness of rectangular oil pad incorporated with random waviness and linear slope on x- and y axes; Fig. 8c is dimensionless film thickness of circular oil pad incorporated with Fourier waviness and linear slope on x coordinate axis; Fig. 8d is dimensionless film thickness of circular oil pad incorporated with random waviness and linear slope on x axis; Fig. 8e is dimensionless film thickness of journal oil pad incorporated with Fourier waviness and linear slope on y axis; Fig. 8f is dimensionless film thickness of journal oil pad incorporated with random waviness and linear slope on y axis. The geometrical error could only be determined from the actual manufacturing conditions, and its verification by additional experimentation is needed.

The numerical pressure distribution is considered as a prerequisite for the analysis of carrying capacity as well as for the geometrical error confirmation. The amount of FDM data transmitted through cloud server is determined by mesh, namely node distribution. For most cases, the numerical calculation for carrying capacity or flow rate is not reliable unless the node number exceeds 2500. A selected portion of the data of pressure distribution and film thickness needed to be transmitted through the cloud platform is shown in Tables 1 and 2.

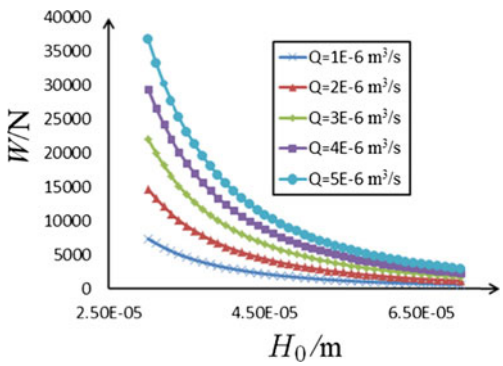

Fig. 9 Variation of carrying capacity of oil films of different thickness

4.2 Experimental verification of the theoretical results

According to Eq. 6, the carrying capacity is highly associated with the dimensionless carrying capacity, dimensionless oil flow rate, film thickness, structure of oil pad, oil viscosity, oil supply rate, etc. The dimensionless carrying capacity and dimensionless flow rate are determined by dimensionless pressure distribution, which is constant for identical oil pads; the geometry of oil pad remains constant while the hydrostatic bearing is working; the variation of oil viscosity could be considered as constant at thermostatic conditions and low speed. Therefore, the carrying capacity is mainly related to film thickness and oil supply rate. For $\overline{W} = 0.6899, \overline{q} = 3.099 \quad , L = 0.5\text{m}, B = 0.1\text{m}, l = 0.45\text{m}, b = 0.05\text{m}, and\, \eta = 0.0174\text{Pa·s}$, the variation of carrying capacity with film thickness and oil supply rate are shown in Fig. 9.

In Fig. 9, the theoretical relationship between carrying capacity, film thickness, and oil supply rate is given, and it will form the basis for further analysis. Verification of the results is necessary before their acceptance. For reasons such as limitations of funding or space, the designer may not able to build an experimental platform himself, so the experiments and adjusting

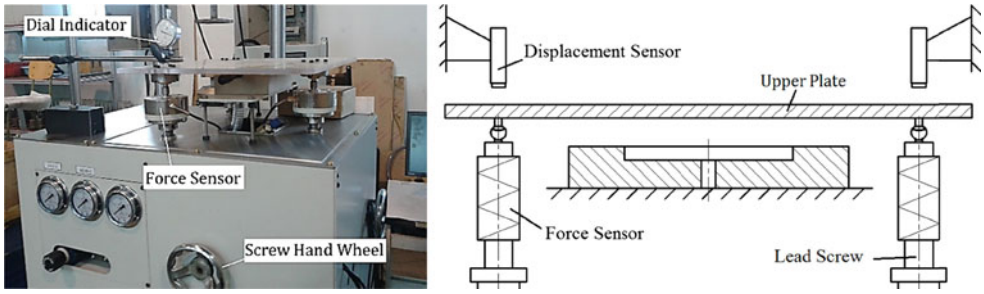

(a) Experimental platform (b) Block diagram

Fig. 10 Experimental platform for determining carrying capacity. **a** Experimental platform. **b** Block diagram

operations are always carried out by the manufacturer. A timely communication platform between the designer and manufacturer is provided by the cloud server, to enable the designer to participate in conducting the experiments and overcoming the problem of geographic distance. An experimental platform for miniature oil pad used for testing in this study is shown in Fig. 10.

A dial indicator as a displacement sensor and three lead screws connected with force sensor were used with the experimental platform. The upper plate could be moved up or down through 2 μm when the screw hand wheel rotated one round. When upper plate came in contact with the oil pad, the dial indicator was set at 0 as a reference for film thickness measurements. The upper plate was moved slightly by lead screw for compensating the elastic deformation of force sensor. The film thickness and supporting force were recorded and transmitted to the designer through the cloud server to check theoretical analysis. For the following values of experimental parameters, $L=0.2\text{m}, B=0.04\text{m}, l=0.18\text{m}, b=0.02\text{m}, \eta=0.0174\text{Pa}\cdot\text{s}, Q_e=3.3\times10^{-6}\text{m}^3/\text{s}$, the comparison of theoretical results and experimental data are shown in Fig. 11:

Figure 11 shows that the trend of variation of theoretical and experimental results corresponds to each other in general. But obvious error occurred when the film thickness was less than 40 μm. This may be due to the supply pump reaching its pressure limit. From the curve fitting results, the dimensionless carrying capacity was determined as $\overline{W}=0.7079$ to match the experimental and theoretical values for ensuring the reliability of the hydrostatic bearing.

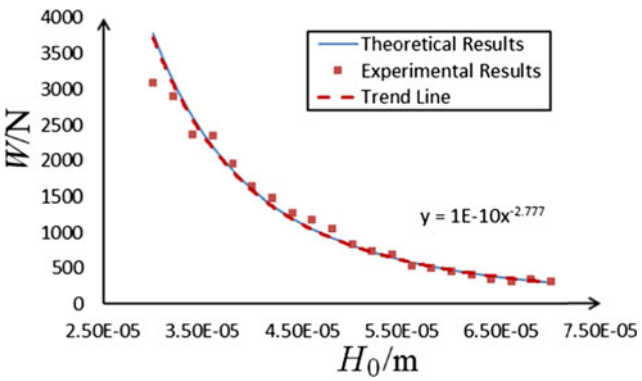

Fig. 11 Comparison between theoretical and experimental results

4.3 Design case of ram bearing

According to the experimental platform shown in Fig. 10 and calibration based on the data in Fig. 11, the targeted analysis for customized hydrostatic bearing is now presented. On the basis of Eq. 6, the carrying capacity of oil pad is associated with the relationship involving reciprocal of film thickness of third degree. Minor variation occurring in film thickness would greatly influence the carrying capacity because it is usually not more than 100 μm in depth. The bearing system of ram is always assembled with several rectangular oil pads fixed face to face. This assembly has strong impact to the precision of the machine tool since the ram handles the tool-holder shaft directly.

In Fig. 12, $H01$ is the film thickness of oil pad 1, $H02$ is the film thickness of oil pad 2, L_r is the width of ram, D_r is the inner width of ram carriage, $W1$ is the carrying force of oil pad 1, $W2$ is the carrying force of oil pad 2, and F_m is the cutting force while machining. As shown in Fig. 12, the ram reaches balance when $W1$, $W2$, and Fm coordinate with each other. When the machine tool is not machining a workpiece, $W1$ is equal to $W2$ and the ram locates at a

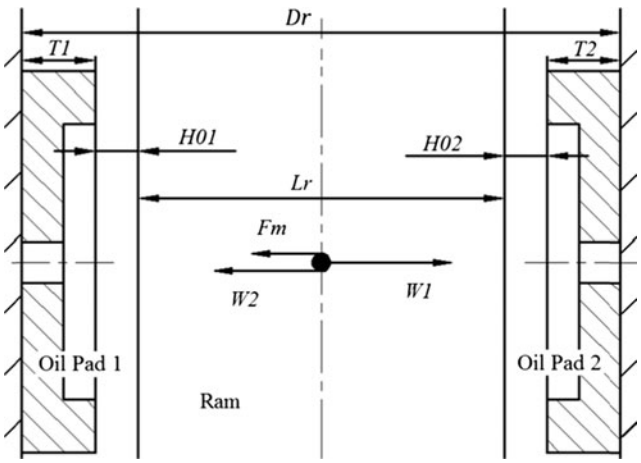

Fig. 12 Oil pads placed face to face for lubrication of ram

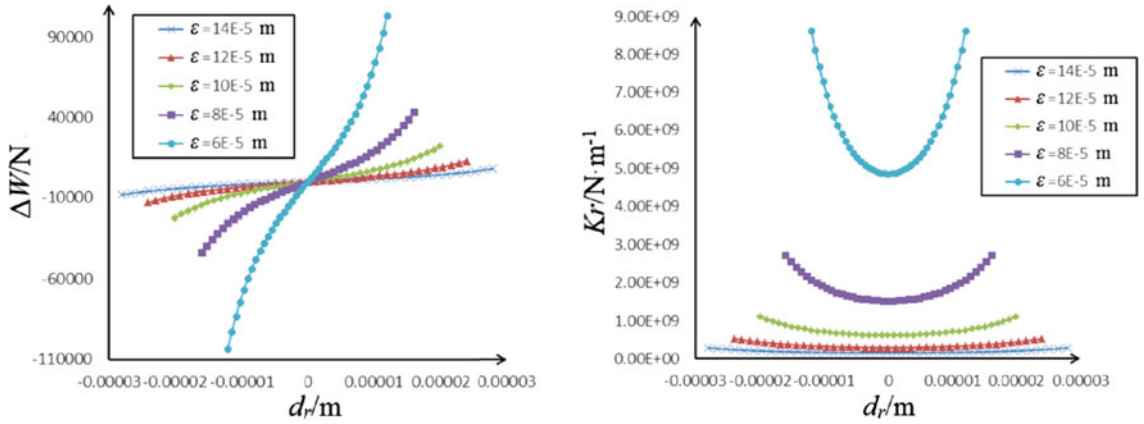

(a) Force difference betweeen the two oil pads (b) Cutting stiffness

Fig. 13 Impact of cutting force on ram for different values of ε. **a** Force difference between the two oil pads. **b** Cutting stiffness

balance point; when cutting a workpiece, the ram will be moved by *F*m in anti-feed direction, which causes machining error. The film thickness on each side of the ram is associated with the size of the ram, ram carriage, and oil pads. Therefore, the working performance of the ram is influenced by its geometrical tolerances. By assuming that the comprehensive gap ε is the sum of their geometrical errors, namely the sum of film thickness of oil pads on both sides, the following relationships are obtained:

$$\begin{cases} W1 = W2 + F_m \\ \varepsilon = H01 + H02 = D_r - L_r - T1 - T2 \end{cases} \quad (7)$$

Equation 7 shows that the comprehensive gap ε influences the machining precision. To meet the consumer's requirements, processing and assembly tolerances of the ram component should be specified by the designer according to FDM analyses as guidelines to the manufacturer. For the following values of oil pad parameters, $\overline{W} = 0.7079, \overline{q} = 3.099, L = 0.5\text{m}$, $B = 0.1\text{m}, l = 0.45\text{m}$, $b = 0.05\text{m}, \eta = 0.0174\text{Pa·s}$, and $Q_e = 3.3 \times 10^{-6}\text{m}^3/\text{s}$, the cutting force resisting ability of ram for different values of ε is shown in Fig. 12:

In Fig. 13, d_r is the ram displacement, ΔW is the force difference between two oil pads, and Kr is the resistant stiffness under the cutting force impact. The greater is ΔW for same value of dr, the stronger is the cutting force resistance ability of ram and also the cutting stiffness. As shown in Fig. 13, the cutting stiffness attains minimum at the balance point. The ram is able to offset any cutting force fluctuation. The extent of ram offset can be limited by an appropriate value of ε. The variation of minimum value of cutting stiffness with ε is shown in Fig. 14.

Based on consumer's requirements, an appropriate value of ε needs to be determined to be used as criteria for machining and assembly by the manufacturers. For instance, it is necessary for the cutting resistance stiffness to be more than 2×10^8 N/m, if the ram is required to move through 10 μm under a cutting force of 2000 N. According to the results shown in Fig. 14, the comprehensive gap should be set as $\varepsilon < 1.124\times10^{-4}$ m to meet the consumer's requirements. The machining parameters transmitted to the manufacturer are shown in Table 3.

5 Conclusions

In this paper, a customized hydrostatic system cloud manufacture model is presented. The functional requirements of a consumer are fulfilled better if all the participants exchange enough data in real time through the cloud server. The prototype model is prepared by a designer according to the consumer's demand, and the machining parameters of essential components of hydrostatic bearing such as oil pads are sent to a manufacturer. The geometrical errors and experimental data

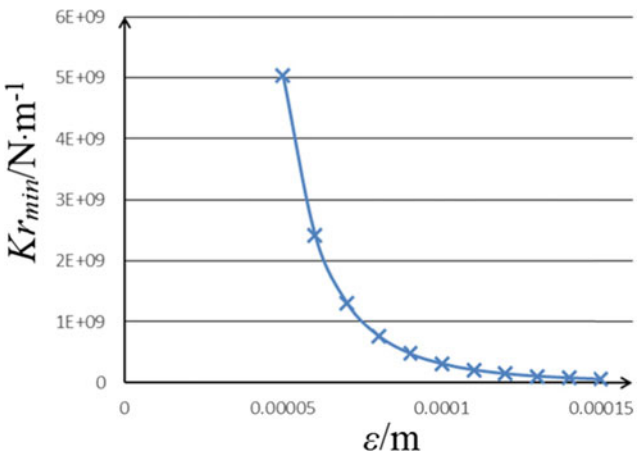

Fig. 14 Variation of cutting resistant stiffness with ε

Table 3 Machining parameters

Parameter	Value/range	Parameter	Value/range
L	0.5 m	l	0.45 m
B	0.1 m	b	0.05 m
ε	$0 \sim 1.124 \times 10^{-4}$m	η	0.0174Pa·s
Qe	3.3×10^{-6}m^3/s	……	

determined by the manufacturer are sent back to the designer to adjust the calculation or verify the theoretical resolution. The monitoring data of hydrostatic system could also be fed back to the designer for performance evaluation.

The following characteristics and advantages of the customized hydrostatic bearing cloud manufacture model were established:

1. A network-based cloud platform was developed for the designer, manufacturer, and consumer of hydrostatic systems and was utilized for communication in real time. The model ensured reliability and efficiency of the product manufactured.
2. The FDM technique was used to analyze the carrying capacity numerically, and the intricate geometrical error was approximated into film thickness to simulate the actual working conditions, by taking advantage of the big data processing ability of cloud server.
3. Information exchange opportunity was extended to all participants at every step of the manufacture to detect and correct the problems in a timely fashion and ensure that the production was under effective control.

Acknowledgments The authors would like to thank the National Science and Technology Major Project coded 2013ZX04013-011, the National Natural Science Fund coded 51575009, and the Jing-Hua Talents Project of Beijing University of Technology for supporting this research.

References

1. Zhang L, Luo Y, Tao F, Bo H, Li LR, Zhang X, Guo H, Cheng Y, Anrui H, Liu Y (2012) Cloud manufacturing: a new manufacturing paradigm. Enterp Inf Syst. doi:10.1080/17517575.2012.683812
2. Tao F, Zhang L, Liu YK, Cheng Y, Wang LH, Xun X (2015) Manufacturing service management in cloud manufacturing: overview and future research directions. J Manuf Sci Eng Trans ASME. doi:10.1115/1.4030510
3. Sharifi H, Colquhoun G, Barclay I, Dann Z (2001) Agile manufacturing: a management and operational framework. Proc Inst Mech Eng B J Eng Manuf 215(6):857–869
4. Meier H, Roy R, Seliger G (2010) Industrial product-service systems—IPS2. CIRP Ann Mfg Technol 59(2):607–627
5. Tao F, Zhang L, Liu Y, Cheng Y, Wang L, Xu X (2015) Manufacturing service management in cloud manufacturing: overview and future research directions. J Manuf Sci Eng 137:040912
6. Tao F, Zhang L, Venkatesh VC, Luo Y, Cheng Y (2011) Cloud manufacturing: a computing and service oriented manufacturing model. Proc IMechE Part B J Eng Manuf 225:1969–1976
7. Tao F, Cheng Y, Zhang L, Nee AYC (2015) Advanced manufacturing systems: socialization characteristics and trends. J Intell Manuf. doi:10.1007/s10845-015-1042-8
8. Tao F, Cheng Y, Xu LD, Lin Z, Li BH (2014) CCIoT-CMfg: cloud computing and internet of things-based cloud manufacturing service system. IEEE Trans Ind Inform 10(2):1435–1442
9. Li J, Tao F, Cheng Y, Zhao L (2015) Big data in product lifecycle management. Int J Adv Manuf Technol 81:667–684
10. Luo Y, Zhang L, Tao F, Ren L, Liu YK, Zhang ZQ (2013) A modeling and description method of multidimensional information for manufacturing capability in cloud manufacturing system. Int J Adv Manuf Technol 69:961–975
11. Tao F, Hu Y, Zhao D, Zhou Z (2009) Study on resource service match and search in manufacturing grid system. Int J Adv Manuf Technol 43:379–399. doi:10.1007/s00170-008-1699-7
12. Tao F, Hu Y, Zhou Z (2007) Study on manufacturing grid and its resource service optimal-selection system. Int J Adv Manuf Technol. doi:10.1007/s00170-007-1033-9
13. Wang L, Wang W, Wang H, Ma T, Hu Y (2014) Numerical analysis on the factors affecting the hydrodynamic performance for the parallel surfaces with microtextures. J Tribol 136(2):021702
14. Meng X, Bai S, Peng X (2014) Lubrication film flow control by oriented dimples for liquid lubricated mechanical seals. Tribol Int 77:132–141
15. Tao F, Zuo Y, Xu LD, Zhang L (2014) IoT-based intelligent perception and access of manufacturing resource toward cloud manufacturing. IEEE Trans Ind Inform 10(2):1547–1557
16. Howe J (2009) Why the power of the crowd is driving the future of business, 1st edn. China CITIC Press, Beijing
17. Qiu MF, Bailey BN, Raeymaekers RSB (2014) The accuracy of the compressible Reynolds equation for predicting the local pressure in gas-lubricated textured parallel slider bearings. Tribol Int 72:83–89
18. Ochoa ED, Otero JE, Lopez AS, Tanarro EC (2015) Film thickness predictions for line contact using a new Reynolds–Carreau equation. Tribol Int 82:133–141
19. Habchi W, Bair S, Qureshi F, Covitch M (2013) A film thickness correction formula for double-newtonian shear-thinning in rolling EHL circular contacts. Tribol Lett 50:59–66
20. Bair SA (2006) Reynolds–Ellis equation for line contact with shear-thinning. Tribol Int 39(4):310–316
21. Khlifi ME (2007) Numerical modeling of non-newtonian fluids in slider bearings and channel thermohydrodynamic flow. J Tribol 129:695–699
22. Cheng Q, Zhao HW, Zhang GJ, Gu PH, Cai LG (2014) An analytical approach for crucial geometric errors identification of multi-axis machine tool based on global sensitivity analysis. Int J Adv Manuf Technol 75(10):107–121
23. Cheng Q, Feng QN, Liu ZF, Gu PH, Cai LG (2014) Fluctuation prediction of machining accuracy for multi-axis machine tool based on stochastic process theory. Proc Inst Mech Eng C J Mech Eng Sci. doi:10.1177/0954406214562633
24. Ji JH, Fu YH, Bi QS (2014) Influence of geometric shapes on the hydrodynamic lubrication of a partially textured slider with micro-grooves. J Tribol 136:041702-1-8
25. Masjedi M, Khonsari MM (2015) On the effect of surface roughness in point-contact EHL: formulas for film thickness and asperity load. Tribol Int 82:228–244
26. Leem CS, Lee HJ (2004) Development of certification and audit processes of application service provider for IT outsourcing. Technovation 24(1):63–71
27. Rosenthal M, Mork P, Li MH, Stanford J, Koester D, Reynolds P (2009) Cloud computing: a new business paradigm for biomedical information sharing. J Biomed Inform 43(2):342–353

28. Li YZ, Zhou K, Zhang Z (2015) A flow-difference feedback iteration method and its application to high-speed aerostatic journal bearings. Tribol Int 84:132–141
29. Nicoletti R (2013) Comparison between a meshless method and the finite difference method for solving the Reynolds equation in finite bearings. J Tribol 135(10):044501-1-9
30. Li J, Chen HS (2007) Evaluation on applicability of Reynolds equation for squared transverse roughness compared to CFD. J Tribol 129(10):963–967
31. Getachew AD, Prawal S (2011) THD analysis for finite slider bearing with roughness: special reference to load generation in parallel sliders. Acta Mech. doi:10.1007/s00707-011-0515-x
32. Tao F, LaiLi Y, Xu L, Zhang L (2013) FC-PACO-RM: a parallel method for service composition optimal-selection in cloud manufacturing system. IEEE Trans Ind Inform 9(4):2023–2033
33. Tao F, Zhao D, Hu Y, Zhou Z (2008) Resource service composition and its optimal-selection based on particle swarm optimization in manufacturing grid system. IEEE Trans Ind Inform 4(4):215–237
34. Wang L (2014) Machine availability monitoring and machining process planning towards cloud manufacturing. CIRP J Manuf Sci Technol 6:263–273
35. de Rafaelli de CC, Lúcia MAD, Yuri F, de Daniel O (2015) Optimizing virtual machine allocation for parallel scientific workflows in federated clouds. Futur Gener Comput Syst 46:51–68